Published in final edited form as:

ACS Sens. 2021 June 25; 6(6): 2225–2232. doi:10.1021/acssensors.1c00124.

In Vivo Platelet Detection Using a Glycoprotein IIb/IIIa-Targeted Near-Infrared Fluorescence Imaging Probe

Khanh Ha[⊥],

Masonic Medical Research Institute, Utica, New York 13501, United States; Center for Systems Biology, Massachusetts General Hospital, Harvard Medical School, Boston, Massachusetts 02114, United States

Xiaoxin Zheng[⊥],

Cardiovascular Research Center, Cardiology Division, Massachusetts General Hospital, Harvard Medical School, Boston, Massachusetts 02114, United States; Present Address: Department of Cardiology, Renmin Hospital of Wuhan University, Cardiovascular Research Institute, Wuhan University, Hubei Key Laboratory of Cardiology, Wuhan, Hubei, China.;

Chase W. Kessinger,

Masonic Medical Research Institute, Utica, New York 13501, United States; Cardiovascular Research Center, Cardiology Division, Massachusetts General Hospital, Harvard Medical School, Boston, Massachusetts 02114, United States

Adam Mauskapf,

Cardiovascular Research Center, Cardiology Division, Massachusetts General Hospital, Harvard Medical School, Boston, Massachusetts 02114, United States

Wenzhu Li,

Cardiovascular Research Center, Cardiology Division, Massachusetts General Hospital, Harvard Medical School, Boston, Massachusetts 02114, United States

Corresponding Authors: **Xiaoxin Zheng –** Cardiovascular Research Center, Cardiology Division, Massachusetts General Hospital, Harvard Medical School, Boston, Massachusetts 02114, United States; Present Address: Department of Cardiology, Renmin Hospital of Wuhan University, Cardiovascular Research Institute, Wuhan University, Hubei Key Laboratory of Cardiology, Wuhan, Hubei, China.; Phone: +86 (027)88041911-82213; xiaoxinzheng@whu.edu.cn; Fax: +86 (027) 88041237; **Farouc A. Jaffer –** Cardiovascular Research Center, Cardiology Division, Massachusetts General Hospital and Wellman Center for Photomedicine, Massachusetts General Hospital, Harvard Medical School, Boston, Massachusetts 02114, United States; Phone: (617) 724-9353; fjaffer@mgh.harvard.edu; Fax: (617) 643-3451; **Jason R. McCarthy –** Masonic Medical Research Institute, Utica, New York 13501, United States; Center for Systems Biology, Massachusetts General Hospital, Harvard Medical School, Boston, Massachusetts 02114, United States; Phone: (315) 624-7478; jmccarthy@mmri.edu; Fax: (315) 735-5648.

Author Contributions

K.H., X.Z., C.W.K., A.M., W.L., and M.O. performed the experiments. K.H., X.Z., S.A.H., F.A.J., and J.R.C. reviewed, analyzed, and interpreted the data. K.H., X.Z., F.A.J., and J.R.C. wrote the paper. All authors discussed the results and commented on the manuscript. F.A.J. and J.R.M. shared senior authorship.

[⊥]K.H. and X.Z. contributed equally to this work.

Supporting Information

The Supporting Information is available free of charge at https://pubs.acs.org/doi/10.1021/acssensors.1c00124.

Synthesis of TIRO-CyAl5.5, inclusive of the compound characterization data, determination of the optimal timing for intravital fluorescence imaging, immunofluorescent microscopy using the platelet-specific CD41 antibody, IF and immunohistochemistry control slides, and flow cytometric analysis of the GPIIb/IIIa activation status (PDF)

Complete contact information is available at: https://pubs.acs.org/10.1021/acssensors.1c00124

The authors declare the following competing financial interest(s): Farouc Jaffer - Sponsored research from Canon, Siemens, Shockwave, and Teleflex; consultant for Boston Scientific, Abbott Vascular, Siemens, Biotronik. Equity interest, Intravascular Imaging Incorporated. Massachusetts General Hospital has a patent licensing arrangement with Canon.

Yoichiro Kawamura,
Cardiovascular Research Center, Cardiology Division, Massachusetts General Hospital, Harvard Medical School, Boston, Massachusetts 02114, United States

Makoto Orii,
Cardiovascular Research Center, Cardiology Division, Massachusetts General Hospital, Harvard Medical School, Boston, Massachusetts 02114, United States

Scott A. Hilderbrand,
Center for Systems Biology, Massachusetts General Hospital, Harvard Medical School, Boston, Massachusetts 02114, United States; Present Address: Dyne Therapeutics, Waltham, Massachusetts, USA.

Farouc A. Jaffer,
Cardiovascular Research Center, Cardiology Division, Massachusetts General Hospital and Wellman Center for Photomedicine, Massachusetts General Hospital, Harvard Medical School, Boston, Massachusetts 02114, United States;

Jason R. McCarthy
Masonic Medical Research Institute, Utica, New York 13501, United States; Center for Systems Biology, Massachusetts General Hospital, Harvard Medical School, Boston, Massachusetts 02114, United States;

Abstract

Platelets play a prominent role in multiple diseases, in particular arterial and venous thrombosis and also in atherosclerosis and cancer. To advance the *in vivo* study of the biological activity of this cell type from a basic experimental focus to a clinical focus, new translatable platelet-specific molecular imaging agents are required. Herein, we report the development of a near-infrared fluorescence probe based upon tirofiban, a clinically approved small-molecule glycoprotein IIb/IIIa inhibitor (GPIIb/IIIa). Through *in vitro* experiments with human platelets and *in vivo* ones in a murine model of deep-vein thrombosis, we demonstrate the avidity of the generated probe for activated platelets, with the added benefit of a short blood half-life, thereby enabling rapid *in vivo* visualization within the vasculature.

Graphical Abstract

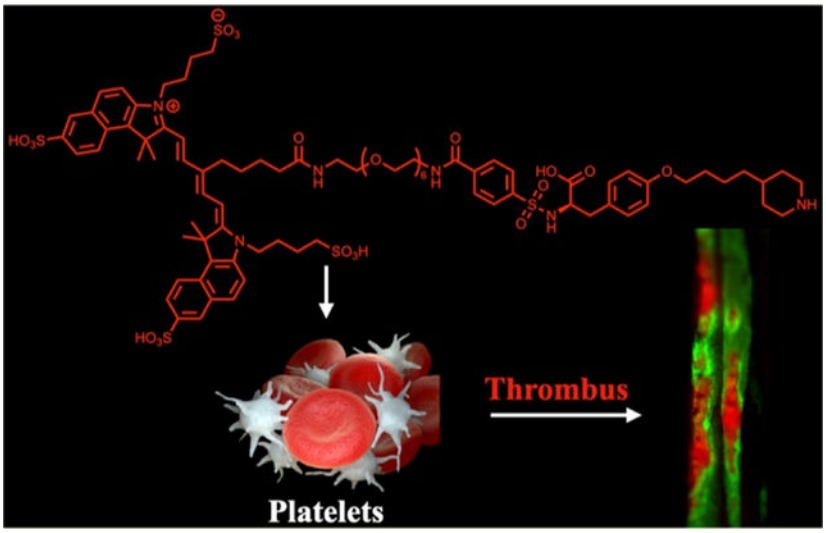

Keywords

near-infrared fluorescence; platelets; in vivo imaging; thrombosis; glycoprotein IIb/IIIa

Platelets play a critical hemostatic role in the prevention of blood loss after injury, initially adhering to the damaged endothelium where they become activated, enabling aggregation and formation of a hemostatic plug, which is subsequently strengthened by fibrin deposition and cross-linking. While this process is lifesaving under conditions of trauma, under pathological conditions, exaggerated platelet-driven thrombosis is a direct cause of significant cardiovascular morbidity and mortality. Most commonly, platelet adhesion, activation, and aggregation are caused as a result of disrupted endothelium, as is observed in the setting of atherosclerotic plaque rupture in myocardial infarction and stroke or following endothelial activation as found in deep-vein thrombosis (DVT).[1,2] Activated platelets are also increasingly recognized for their pathophysiologic role in cancer, where they promote tumorigenesis, angiogenesis, and metastasis.[3]

Although platelets may be activated through a number of different pathways, including thrombin- and collagen-mediated mechanisms, each converges upon a shared pathway, which results in the upregulation of integrins, leading to increased interactions between platelets, platelets and other cell types, and platelets and the extracellular matrix.[4] Of these receptors, P-selectin and glycoprotein IIb/IIIa (GPIIb/IIIa) are the most abundant, with the GPIIb/IIIa receptor being further exposed under conditions of thrombosis and platelet activation.[5] The former is responsible for the interactions between platelets, leukocytes, and endothelial cells, while the latter is the driving force behind platelet aggregation. Other integrins, including $\alpha 2\beta 1$, $\alpha 5\beta 1$, $\alpha 6\beta 1$, and $\alpha v\beta 3$, are responsible for the binding of platelets to collagen, fibronectin, laminin, and vitronectin, respectively.

The ability to characterize activated platelets *in vivo* at cellular-level resolution through intravital microscopy (IVM) of the fluorescently labeled cells allows for assessment of their response to a variety of disease states.[6] Historically, clinically translatable molecular

imaging approaches for platelets have utilized nuclear imaging, ultrasound (US), or magnetic resonance imaging (MRI). However, these noninvasive approaches lack the ability to detect platelets at high resolution. In contrast, imaging at the microscopic level is feasible through fluorescence imaging, but new imaging agents are required beyond the previously detailed examples utilizing long-circulating antibodies.[7–10] In addition, for translation to human coronary artery disease, near-infrared fluorescence (NIRF) molecular imaging enables high-resolution, clinical-type imaging through intravascular NIRF catheters.[11,12] Fluorescence imaging thus offers a bench-to-bedside opportunity for platelet-targeted molecular imaging.[13]

To more rapidly translate our NIRF molecular imaging efforts of platelets into the clinical arena, instead of investigating *de novo* targeting ligands for the detection of activated platelets, we re-engineered compounds clinically used for the prevention of platelet aggregation, namely, GPIIb/IIIa inhibitors, molecules that block the final common pathway of platelet aggregation.[2] We initially considered all three clinical GPIIb/IIIa agents, including the human–murine chimeric monoclonal antibody Fab fragment abciximab, with a dissociation constant (K_d) of 5 nM; the small-molecule tirofiban RGD mimetic, with a K_d of 15 nM; and the heptapeptide RGD mimetic eptifibatide, with a K_d of 120 nM.[14] A near-infrared fluorophore-labeled probe should possess a short blood half-life to enable rapid *in vivo* investigation of the platelet activation status and would induce only a negligible impact on platelet aggregation. Tirofiban was ultimately chosen for this study, as the high affinity, low dissociation constant, and prolonged antiplatelet effect of abciximab decrease its attractiveness as a diagnostic imaging agent. Additionally, tirofiban, compared to eptifibatide, shows similar pharmacokinetics, yet tirofiban possesses an eightfold greater affinity for the target receptors on platelets. Previously, polyethylene glycol (PEG)-modified analogues of tirofiban were investigated for their capabilities as cryoprotective agents for the storage of frozen platelets.[15] These prior studies demonstrated that depending upon the polymer's size appended to the parent molecule, the alkyl chain adjacent to the sulfonamide group in tirofiban could readily be replaced with the molecule, retaining its ability to prevent platelet aggregation.

RESULTS AND DISCUSSION

Probe Design and Synthesis.

We set out to synthesize a novel tirofiban analogue bearing a near-infrared fluorophore spatially separated with a discrete PEG linker, in an attempt to ensure that the sterically bulky dye did not affect the binding affinity of the drug moiety. Using a modification of the synthetic strategy initially developed by Chung *et al.*,[16] we replaced the alkyl chain in the parent molecule with benzoic acid, enabling a conjugatable handle for further modification (Scheme 1). Reduction of carboxylic acid **1** with lithium aluminum hydride afforded piperidinyl butanol **2**, the secondary amine of which was subsequently protected, allowing for bromination of the alcohol **3** with CBr_4 in the presence of PPh_3 to give compound **4**. This intermediate was then used to alkylate *N*-benzyloxycarbonyl-*O*-*tert*-butyl-L-tyrosine to provide fully protected **5**. Cbz deprotection and sulfonylation of the resulting free amine **6** with 4-(chlorosulfonyl)benzoic acid gave the modified tirofiban analogue **7**.

Concomitant with the ligand synthesis, we generated a NIR fluorophore-labeled PEG_6 bearing a terminal amine. Using a modification of the high-yielding, one-pot synthesis previously described by us for the synthesis of symmetric cyanine dyes,[17] we synthesized CyAl5.5 in 29% yield. To the succinimidyl ester of this dye was subsequently conjugated *t*-Boc-*N*-amido-PEG_6-amine, which was further deprotected to give the CyAl5.5-*N*-amido-PEG_6-amine. The final conjugation of the PEG-modified dye to **7** was hindered by the poor reactivity of the carboxylic acid moiety on the ligand. We attempted this amide bond formation in one step using 1-ethyl-3-(3-dimethylaminopropyl)carbodiimide, *N*-ethoxycarbonyl-2-ethoxy-1,2-dihydroquinoline, or benzotriazol-1-yl-oxytripyrro-lidinophosphonium hexafluorophosphate in the presence of a base or *via* the formation and subsequent reaction of the succinimidyl ester of **7**, each with negligible yields. Ultimately, conjugation was afforded by activation of the carboxylic acid with 2-(1*H*-benzotriazol-1-yl)-1,1,3,3-tetramethyluronium hexafluorophosphate to give the penultimate product in 28% yield, which was then deprotected with trifluoroacetic acid in dichloromethane to give the final imaging agent, TIRO-CyAl5.5.

In Vitro Binding of TIRO-CyAl5.5 to Human Platelets.

In vitro validation of binding and imaging efficacy was accomplished using human platelet suspensions. The platelets were incubated with TIRO-CyAl5.5 and free CyAl5.5 or were pre-incubated with the clinically utilized GPIIb/IIIa inhibitor tirofiban to induce a blockade of the receptors and were pelleted and imaged using fluorescence reflectance imaging (FRI).[18] As is shown in Figure 1, the fluorescence signal (target-to-background ratio, TBR) for the TIRO-CyAl5.5 was twofold higher than that of free CyAl5.5 (TBR 4.23 ± 1.03 *vs* 2.13 ± 0.38, $P < 0.05$), while pre-incubation with unlabeled tirofiban diminished the binding of TIRO-CyAl5.5 in a dose-dependent manner (TBR 3.09 ± 0.63 for molar equivalent dose, 2.14 ± 0.59 and 2.09 ± 0.43 for 10-fold excess and 100-fold excess, respectively, Figure 1). Interestingly, unconjugated CyAl5.5 slightly bound with platelets, as demonstrated by its baseline NIRF signal enhancement, possibly attributable to nonspecific binding under *in vitro* conditions without blood flow. Altogether, these results suggest that TIRO-CyAl5.5 binds specifically to the GPIIb/IIIa receptor, similar to unlabeled tirofiban, demonstrating that any structural changes induced by the modification of the parent compound do not significantly hinder its capabilities as a platelet-targeted imaging agent.

Plasma Elimination Half-Life and *In Vivo* Biodistribution Studies of TIRO-CyAl5.5.

Initial *in vivo* experimentation focused upon the determination of the plasma elimination half-life for TIRO-CyAl5.5, as rapid blood pool clearance is necessary for intravascular NIRF imaging applications in the cardiac catheterization laboratory, where patients would be injected with molecular imaging agents during the procedure. In these experiments (Figure 2), the imaging agent TIRO-CyAl5.5 was delivered *via* a 10 nmol/kg intravenous bolus into naïve C57BL/6J mice ($N = 6$); serial blood collection was accomplished *via* the carotid artery, and the NIRF signal was measured *via* FRI. As anticipated, the blood pool NIRF signal decreased rapidly, revealing a relatively short blood half-life of 5.65 min (95% CI, 4.54–7.47).

We next assessed the biodistribution of the agent, as compared to that of the free dye, in a model of $FeCl_3$-induced venous thrombosis.[19] This model has been utilized extensively to elicit platelet-rich thrombi *via* the chemical-induced injury of the vascular endothelium and subsequent recruitment and aggregation of activated platelets (CD41 staining, Figure S2).[20–23] TIRO-CyAl5.5 or CyAl5.5 was injected into its respective cohort of mice and allowed to circulate for 30 min prior to sacrifice. The organs were removed, and the fluorescence TBR for each organ was determined by FRI. While the NIRF signal from the lung, liver, and kidney demonstrated significant accumulation of both TIRO-CyAl5.5 and CyAl5.5, the localization to the jugular vein thrombus for the TIRO-CyAl5.5 was almost threefold higher than that of the free dye (Figure 3).

TIRO-CyAl5.5 Enables *In Vivo* Detection of Platelet-Rich Thrombi.

In vivo detection of platelets was next investigated using the $FeCl_3$-induced femoral DVT model. To enable high-resolution imaging of the thrombus, intravital fluorescence microscopy (IVFM) was utilized in conjunction with a fluorescein conjugate of high-molecular weight dextran to render a fluorescence angiogram of the vessel (Figure 4). In the femoral vein, the fluorescein signal demarcates the vessel lumen, with filling defects demonstrating the outline of thrombi. Initial investigations assessed the most appropriate time to conduct the subsequent determination of targeting efficiency, with 30 min chosen to be ideal based on visual assessment of the thrombus TBR signal (Figure S1). Using this time point, we then compared the platelet thrombus imaging capabilities of TIRO-CyAl5.5 to those of free CyAl5.5 with pre-treatment with a 2500-fold excess of unmodified tirofiban before the injection of TIRO-CyAl5.5. Thrombus TBR ratios were calculated for each of the conditions, with the targeted agent TIRO-CyAl5.5 demonstrating a TBR of 1.9 ± 0.2, which was reduced to 1.3 ± 0.1 ($P < 0.05$) in the competitive blocking group. The free dye (CyAl5.5) exhibited a TBR of 0.9 ± 0.1 *in vivo*, showing minimal nonspecific binding to platelet-rich thrombi (Figure 4D, $P < 0.001$).

Effect of TIRO-CyAl5.5 on Thrombus Length and Volume.

To assess the potential therapeutic effect on thrombus formation by TIRO-CyAl5.5, which is to be avoided for diagnostic imaging agents, the size of the venous thrombi after injection of the agents was calculated for the TIRO-CyAl5.5 and PBS groups. TIRO-CyAl5.5 was given at the imaging dose of 10 nmol/kg of body weight, which is approximately sixfold less than the previously reported murine therapeutic dose of tirofiban.[21]

Anatomical analyses exhibited no significant changes in thrombus length or area between groups (length, 2.02 ± 0.08 *vs* 1.95 ± 0.12 mm, $P > 0.05$; area, 0.24 ± 0.01 *vs* 0.26 ± 0.03 mm^2, $P > 0.05$, Figure 5), demonstrating that TIRO-CyAl5.5 did not induce a significant anti-thrombotic therapeutic effect *in vivo*. Immunofluorescent staining of the thrombi further validated the co-localization of our fluorescent probe to platelets (Figure 6). In contrast, there was little intra-thrombus accumulation either in the control group receiving excess tirofiban to elicit the blocking of GPIIb/IIIa or in the group receiving the free dye (CyAl5.5). While these blocking studies do not preclude the imaging agent binding to other positions on the platelet, given the GPIIb/IIIa-specific nature of the tirofiban molecule,[24]

the abrogation of the intrathrombus accumulation intimates that TIRO-CyAl5.5 binds mainly through GPIIb/IIIa-mediated mechanisms.

CONCLUSIONS

Over the past decade, several groups have investigated the generation of molecular imaging agents capable of visualizing and quantifying platelet aggregation *in vivo*. These probes each used antibody-modified materials to affect contrast in the nuclear, MRI, or US-based detection of thrombosis.[7–10] While these noninvasive strategies demonstrated utility in their described applications, they are limited in their sensitivity and resolution, making the detection of sparse numbers of target cells, such as those observed on coronary plaques or stents, difficult.

Here, we have shown that a new NIR fluorescence molecular imaging agent based upon the clinically utilized GPIIb/IIIa receptor inhibitor tirofiban is capable of binding to and detecting platelets both *in vitro* using human platelets and *in vivo* in a murine model of venous thrombosis. The short blood half-life and the high TBR ratio of the probe enable its utility in many applications where activated platelets are a hallmark of disease. Significant future interests include the catheter-based intravascular NIRF detection of platelets, potentially in the clinical setting, and the investigation of the utility of this probe in other diseases, including cancers, where platelet activation is relevant to disease initiation and progression.

EXPERIMENTAL SECTION

Reagents were purchased from Sigma-Aldrich and used as received. All experimental procedures were approved by the IACUC/Subcommittee on Research Animal Care at Massachusetts General Hospital. Full experimental procedures and methods are provided in the Supporting Information.

In Vitro Binding of TIRO-CyAl5.5 to Human Platelets.

Human platelet-rich plasma (PRP) was obtained using an IRB-approved human subject protocol (#2011B000386). Each platelet pellet was washed and collected from 250 μL of human PRP (Platelet concentration: 2.75×10^8 cells/mL) in HEPES-buffered tyrode (Cat#: 40120241–1, Bio-world, OH, USA) *via* centrifugation at 1000*g* for 5 min. Each platelet pellet was then resuspended and incubated in 1 mL of HEPES-buffered tyrode with 0.01 U thrombin (Cat#: 7593, BioVision, Inc., California, USA) at 37 °C for 15 min. Removal of the citrate buffer *via* washing and treatment with thrombin results in the upregulation of GPIIb/IIIa (Figure S4). After that, 1.2 nmol/mL fluorophore was added to each resuspended sample and incubated at 37 °C for 30 min. In competitive binding assays, pure tirofiban (Cat#: 144494-65-5, Sigma-Aldrich, MO, USA) at the same concentration, 10-fold or 100-fold excess concentration, was added 15 min before the incubation of TIRO-CyAl5.5 with the sample. Each sample was then washed twice and resuspended with HEPES-buffered tyrode. Platelet pellets were then resuspended in 120 μL of HEPES-buffered tyrode, transferred to the corresponding well of the 96-well plate, and imaged by FRI immediately (excitation/emission; 675 nm/695 nm). Experiments were performed in triplicate. Flow

cytometry was accomplished using both the HEPES-buffered tyrode-washed (naïve) and thrombin-treated platelets. The cells were incubated with a FITC-labeled anti-CD41/61 antibody (PAC-1, Biolegend) for 30 min in the dark and then subject to flow cytometry (BD LSRFortessa). Results were analyzed using FACSDiva software, version 6.1.3.

Animal Studies.

All experimental procedures were approved by the IACUC/Subcommittee on Research Animal Care at Massachusetts General Hospital. For *in vivo* studies, C57BL/6J mice (Jackson Laboratory) were anesthetized with an intraperitoneal injection of ketamine and xylazine (80/12 mg/kg). Surgical procedures utilized a stereo zoom microscope. No qualitative differences in feeding, sleeping, drinking, or activity were apparent.

Blood Half-Life Study of TIRO-CyAl5.5.

To determine the elimination blood half-life of TIRO-CyAl5.5, serial blood sampling was performed at 1, 4, 15, 30, 60, 120, and 240 min through the carotid artery, with an artery clamp that was used to block blood after each sampling. C57BL/6J mice ($n = 6$) received a 10 nmol/kg iv bolus of the TIRO-CyAl5.5 dissolved in PBS. At the desired time point, blood of 50 μL volume was obtained and mixed with 50 μL of heparin (1000 USP units/mL) and kept on ice until analysis. The CyAl5.5 NIRF fluorescence of the blood at each time point was imaged by FRI (Kodak Carestream—see other papers for details).[18,25] The blood NIRF signal at each time point was measured and then normalized to the NIRF signal at one-minute post-injection. Exponential fitting using a one-phase decay model yielded the blood half-life of TIRO-CyAl5.5 (GraphPad Prism 5.0, San Diego, CA).

Creation of Venous Thrombosis in Mice.

Ferric chloride ($FeCl_3$)-induced VT was provoked in the jugular or femoral vein of C57BL/6J as described previously.[26] Under anesthesia, the respective vein was surgically exposed; then, a filter paper (Whatman no. 1) soaked in 7.5% $FeCl_3$ was applied to the anterior surface of the vein for 5 min. Thereafter, the filter paper was removed, and the surgical field was thoroughly rinsed with PBS three times.

In Vivo Biodistribution of TIRO-CyAl5.5.

For these experiments, the jugular vein was utilized for the creation of the thrombus. TIRO-CyAl5.5 or free CyAl5.5 was injected 5 min after DVT induction. Thirty minutes later, mouse organs (jugular vein, heart, lung, liver, kidney, spleen, muscle, and bone) were resected and imaged using FRI. A total of 10 mice were studied ($n = 5$ and $n = 5$ for TIRO-CyAl5.5 and free CyAl5.5, respectively).

Intravital Microscopy.

To image platelet deposition in femoral vein thrombi at high resolution, IVM of venous thrombosis was performed ($n = 27$ mice) as previously demonstrated.[7,8,26] Mice were anesthetized as mentioned above. At 5 min after DVT induction (30 min before imaging), TIRO-CyAl5.5 ($n = 9$) or control agent (free CyAl5.5, $n = 8$) was administered *via* retro-orbital injection. Agents were injected at a dose of 10 nmol/kg in 100 μL total volume.

For *in vivo* blocking experiments ($n = 10$), pure tirofiban (25,000 nmol/kg) or PBS was injected 1 min before injection of TIRO-CyAl5.5 (10 nmol/kg). Anesthetized mice were intravenously injected with fluorescent isothiocyanate-conjugated dextran (FITC-dextran, MW: 2,000,000, excitation/emission; 490 nm/520 nm, 5 mg/mL, Sigma, St Louis, MO, USA) to provide angiograms. IVFM studies employed a multichannel laser scanning fluorescence microscope optimized for intravital imaging. All image settings were kept constant for all time points and samples.

Effect of TIRO-CyAl5.5 on Thrombus Length and Volume.

Thrombus length and volume were measured *in vivo* using IVM of femoral VT. TIRO-CyAl5.5 ($n = 8$) was administered *via* retro-orbital injection as mentioned above; 100 μL of PBS was taken as a control agent ($n = 7$). Thirty minutes after TIRO-CyAl5.5 injection (35 min after DVT creation), FITC-dextran was intravenously injected immediately before imaging to provide angiograms and quantification of the venous thrombosis area.[9] IVM studies employed a multichannel laser scanning fluorescence microscope optimized for intravital imaging. All image settings were kept constant for all time points and samples.

Fluorescence Reflectance Imaging.

Human PRP suspension, resected jugular veins, and organs underwent FRI with a NIR filter set (excitation/emission 630/700 nm, Kodak ImageStation 4000, Carestream Health, Inc., Rochester, NY). Multiple exposure times (2–64 s) generated images that were exported to 16-bit unscaled TIFF files for further analysis with ImageJ (version 1.44o, Bethesda, MD).[10] For blood half-lives, samples underwent FRI on another system equipped with a NIR filter set (excitation/emission; 675 nm/695 nm, Odyssey CLx Imaging System, LI-COR Biotechnology, NE, USA). Images were exposed for 6 min, acquired, and exported to zip files for further analysis with Image Studio Lite (version 5.2.5, LI-COR Biotechnology).

Image Analyses.

All image analysis utilized ImageJ or Image Studio Lite software. Thrombi presented as filling defects on FITC-dextran-generated angiograms. Briefly, the adjacent healthy vein and the thrombosed area were automatically stitched together to create one large image stack of the entire thrombosed vein (ImageJ plugin). Regions of interest (ROIs) of the thrombus and the adjacent normal vessel were manually traced. Target-to-background ratios (TBRs) were defined as (mean ROI signal of the target)/(mean ROI signal of the background); the background included the PBS-treated platelet suspension, adjacent femoral vein, jugular vein, and heart.

Histopathology.

After sacrifice, mice were perfused with 0.9% saline (10 mL) *via* the left ventricle. Thrombosed veins were carefully embedded in optimal-cutting temperature (Sakura Finetek, Torrance, CA) media and flash-frozen using a dry ice/isopentane slurry. Cryosections of 6 μm were cut for fluorescence microscopy and all histological analyses. NIR fluorescence microscopy was performed on fresh-frozen femoral vein sections using an upright epifluorescence microscope (Nikon Eclipse 90i, Tokyo, Japan). Fluorescence images

were obtained in the NIR channel for TIRO-CyAl5.5 (excitation/emission; 675 nm/695 nm, exposure time 900 msec) and FITC channel for autofluorescence (excitation/emission; 480 nm/535 nm, exposure time 200 ms). The identical femoral vascular sections were used for IF to visualize the GPIIb/IIIa expression (Figure 6, sheep anti-human platelets GPIIb/IIIa, SA2B3A-IG, Affinity Biologicals) or CD41 expression (Figure S2, purified rat anti-mouse CD41, Clone MWReg30, BD Pharmingen). Adjacent sections were stained with immunohistochemistry to visualize the GPIIb/IIIa expression; Carstairs' and hematoxylin and eosin staining were performed for thrombus assessment and general morphology, respectively. Control sections were processed with the primary antibody omitted.

Statistical Analysis.

Results are reported as mean ± SD. Statistical analysis was performed with GraphPad Prism (Version 5.0, San Diego, CA). Statistical comparisons between two groups were evaluated by the Mann–Whitney *U* test and by the Kruskal–Wallis test for multiple groups, followed by Dunn's post-test. *P* values less than 0.05 were considered statistically significant.

Supplementary Material

Refer to Web version on PubMed Central for supplementary material.

ACKNOWLEDGMENTS

This work was supported in part by the National Institute of Health grants R01HL133153 (J.R.M.), R01HL122238 (J.R.M.), R01HL122388 (F.A.J), R01HL137913 (F.A.J.), R01HL150538 (F.A.J.), and R01HL144550 (subcontracts to F.A.J. and J.R.M.) and the National Natural Science Foundation of China 81800431 (X.Z.).

REFERENCES

(1). Mackman N Triggers Targets and Treatments for Thrombosis. Nature 2008, 451, 914–918. [PubMed: 18288180]

(2). Jackson SP Arterial Thrombosis-Insidious, Unpredictable and Deadly. Nat. Med 2011, 17, 1423–1436. [PubMed: 22064432]

(3). Schlesinger M Role of Platelets and Platelet Receptors in Cancer Metastasis 06 Biological Sciences 0601 Biochemistry and Cell Biology. J. Hematol. Oncol 2018, 11, 125. [PubMed: 30305116]

(4). Yun S-H; Sim EH; Goh RY; Park JI; Han JY Platelet Activation: The Mechanisms and Potential Biomarkers. BioMed Res. Int 2016, 2016, 9060143.

(5). Shattil SJ; Hoxie JA; Cunningham M; Brass LF Changes in the Platelet Membrane Glycoprotein IIb.IIIa Complex during Platelet Activation. J. Biol. Chem 1985, 260, 11107–11114. [PubMed: 2411729]

(6). Bellido-Martín L; Chen V; Jasuja R; Furie B; Furie BC Imaging Fibrin Formation and Platelet and Endothelial Cell Activation in Vivo. Thromb. Haemostasis 2011, 105, 776. [PubMed: 21437353]

(7). Shim CY; Liu YN; Atkinson T; Xie A; Foster T; Davidson BP; Treible M; Qi Y; López JA; Munday A; Ruggeri Z; Lindner JR Molecular Imaging of Platelet-Endothelial Interactions and Endothelial von Willebrand Factor in Early and Mid-Stage Atherosclerosis. Circ. Cardiovasc. Imag 2015, 8, No. e002765.

(8). von Elverfeldt D; Meißner M; Peter K; Paul D; Meixner F; Neudorfer I; Merkle A; Harloff A; Zirlik A; Schöllhorn J; Markl M; Hennig J; Bode C; von zur Muhlen C An Approach towards Molecular Imaging of Activated Platelets Allows Imaging of Symptomatic Human Carotid Plaques in a New Model of a Tissue Flow Chamber. Contrast Media Mol. Imaging 2012, 7, 204–213. [PubMed: 22434633]

(9). Yap ML; McFadyen JD; Wang X; Zia NA; Hohmann JD; Ziegler M; Yao Y; Pham A; Harris M; Donnelly PS; Hogarth PM; Pietersz GA; Lim B; Peter K Targeting Activated Platelets: A Unique and Potentially Universal Approach for Cancer Imaging. Theranostics 2017, 7, 2565–2574. [PubMed: 28819447]

(10). Heidt T; Ehrismann S; Hövener JB; Neudorfer I; Hilgendorf I; Reisert M; Hagemeyer CE; Zirlik A; Reinöhl J; Bode C; Peter K; Von Elverfeldt D; Von Zur Muhlen C Molecular Imaging of Activated Platelets Allows the Detection of Pulmonary Embolism with Magnetic Resonance Imaging. Sci. Rep 2016, 6, 25044. [PubMed: 27138487]

(11). Yoo H; Kim JW; Shishkov M; Namati E; Morse T; Shubochkin R; McCarthy JR; Ntziachristos V; Bouma BE; Jaffer FA; Tearney GJ Intra-Arterial Catheter for Simultaneous Microstructural and Molecular Imaging in Vivo. Nat. Med 2011, 17, 1680–1684. [PubMed: 22057345]

(12). Bozhko D; Osborn EA; Rosenthal A; Verjans JW; Hara T; Kellnberger S; Wissmeyer G; Ovsepian SV; McCarthy JR; Mauskapf A; Stein AF; Jaffer FA; Ntziachristos V Quantitative Intravascular Biological Fluorescence-Ultrasound Imaging of Coronary and Peripheral Arteries in Vivo. Eur. Heart J. Cardiovasc. Imag 2017, 18, 1253–1261.

(13). Ughi GJ; Wang H; Gerbaud E; Gardecki JA; Fard AM; Hamidi E; Vacas-Jacques P; Rosenberg M; Jaffer FA; Tearney GJ Clinical Characterization of Coronary Atherosclerosis With Dual-Modality OCT and Near-Infrared Autofluorescence Imaging. JACC Cardiovasc. Imag 2016, 9, 1304–1314.

(14). Hashemzadeh M; Furukawa M; Goldsberry S; Movahed MR Chemical Structures and Mode of Action of Intravenous Glycoprotein IIb/IIIa Receptor Blockers: A Review. Exp. Clin. Cardiol 2008, 13, 192. [PubMed: 19343166]

(15). Désaubry L; Riché S; Laeuffer P; Cazenave J-P Synthesis and Biological Evaluation of PEG-Tirofiban Conjugates. Bioorg. Med. Chem. Lett 2008, 18, 2028–2031. [PubMed: 18304813]

(16). Chung JYL; Zhao D; Hughes DL; Grabowski EJJ A Practical Synthesis of Fibrinogen Receptor Antagonist MK-383. Selective Functionalization of (S)-Tyrosine. Tetrahedron 1993, 49, 5767–5776.

(17). Shao F; Yuan H; Josephson L; Weissleder R; Hilderbrand SA Dyes and Pigments Facile Synthesis of Monofunctional Pentamethine Carbocyanine Fluorophores. Dyes Pigm 2011, 90, 119–122. [PubMed: 21475610]

(18). Hara T; Ughi GJ; McCarthy JR; Erdem SS; Mauskapf A; Lyon SC; Fard AM; Edelman ER; Tearney GJ; Jaffer FA Intravascular Fibrin Molecular Imaging Improves the Detection of Unhealed Stents Assessed by Optical Coherence Tomography in Vivo. Eur. Heart J 2017, 38, 447–455. [PubMed: 26685129]

(19). Hara T; Bhayana B; Thompson B; Kessinger CW; Khatri A; McCarthy JR; Weissleder R; Lin CP; Tearney GJ; Jaffer FA Molecular Imaging of Fibrin Deposition in Deep Vein Thrombosis Using Fibrin-Targeted near-Infrared Fluorescence. JACC Cardiovasc. Imag 2012, 5, 607–615.

(20). Barr JD; Chauhan AK; Schaeffer GV; Hansen JK; Motto DG Red Blood Cells Mediate the Onset of Thrombosis in the Ferric Chloride Murine Model. Blood 2013, 121, 3733–3741. [PubMed: 23343833]

(21). Flaumenhaft R; Tanaka E; Graham GJ; De Grand AM; Laurence RG; Hoshino K; Hajjar RJ; Frangioni JV Localization and Quantification of Platelet-Rich Thrombi in Large Blood Vessels with near-Infrared Fluorescence Imaging. Circulation 2007, 115, 84–93. [PubMed: 17179017]

(22). Stalker TJ Mouse Laser Injury Models: Variations on a Theme. Platelets 2020, 31, 423–431. [PubMed: 32297542]

(23). Polak D; Talar M; Watala C; Przygodzki T Intravital Assessment of Blood Platelet Function. A Review of the Methodological Approaches with Examples of Studies of Selected Aspects of Blood Platelet Function. Int. J. Mol. Sci 2020, 21, 8334.

(24). Mcclellan KJ; Goa KL; Peerlinck K; Biology V; Théroux P; Heart M Tirofiban. A Review of Its Use in Acute Coronary Syndromes. Drugs 1998, 56, 1067–1080. [PubMed: 9878994]

(25). Verjans JW; Osborn EA; Ughi GJ; Calfon Press MA; Hamidi E; Antoniadis AP; Papafaklis MI; Conrad MF; Libby P; Stone PH; Cambria RP; Tearney GJ; Jaffer FA Targeted Near-Infrared Fluorescence Imaging of Atherosclerosis: Clinical and Intracoronary Evaluation of Indocyanine Green. JACC Cardiovasc. Imag 2016, 9, 1087–1095.

(26). Claessen BE; Henriques JPS; Jaffer FA; Mehran R; Piek JJ; Dangas GD Stent Thrombosis: A Clinical Perspective. JACC Cardiovasc. Interv 2014, 7, 1081–1092. [PubMed: 25341705]

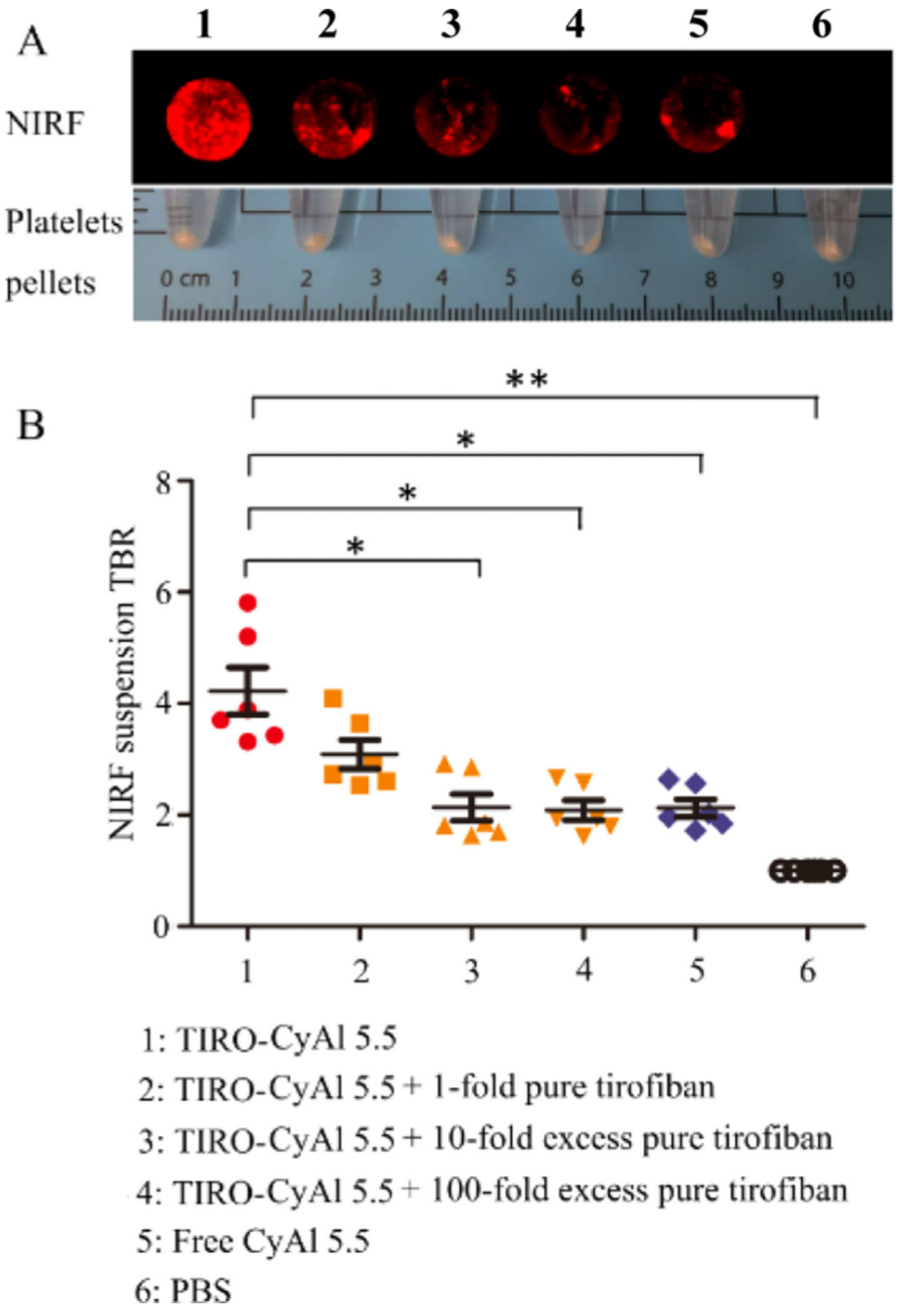

Figure 1.

NIRF targeted imaging of human platelets and competitive inhibition studies. (A) *In vitro* binding affinity of TIRO-CyAl5.5 to human platelets as obtained by FRI. (B) NIRF signal was significantly blocked with an excess of competitor Tirofiban. $*P < 0.05$, $**P < 0.001$.

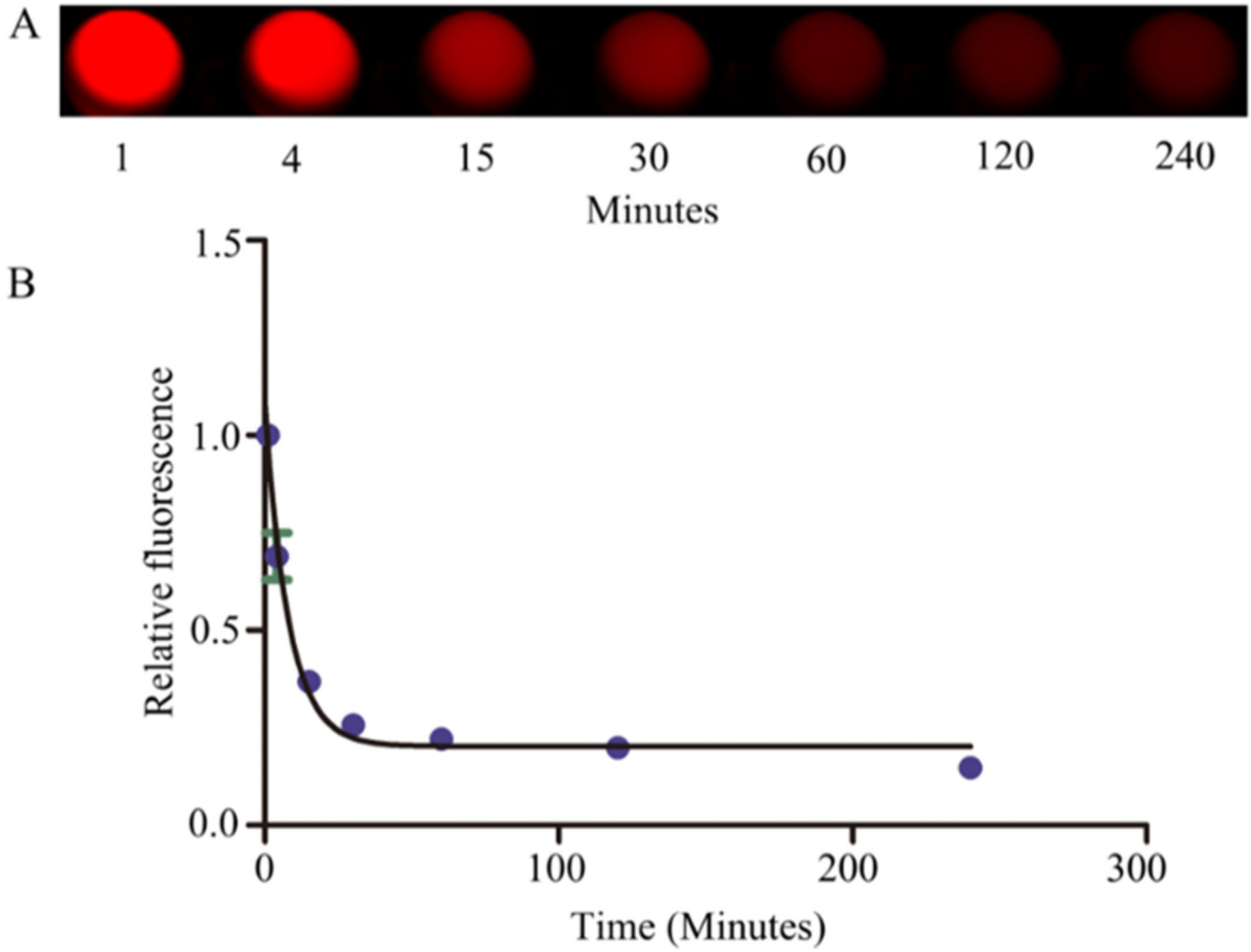

Figure 2.

Determination of the plasma elimination half-life of TIRO-CyAl5.5. After injecting TIRO-CyAl5.5 *via* the tail vein in normal C57BL/6J mice, serial blood sampling was performed *via* the carotid artery and (A) CyAl5.5 levels were measured by NIRF imaging. (B) Blood half-life was 5.65 min (95% CI, 4.54–7.47).

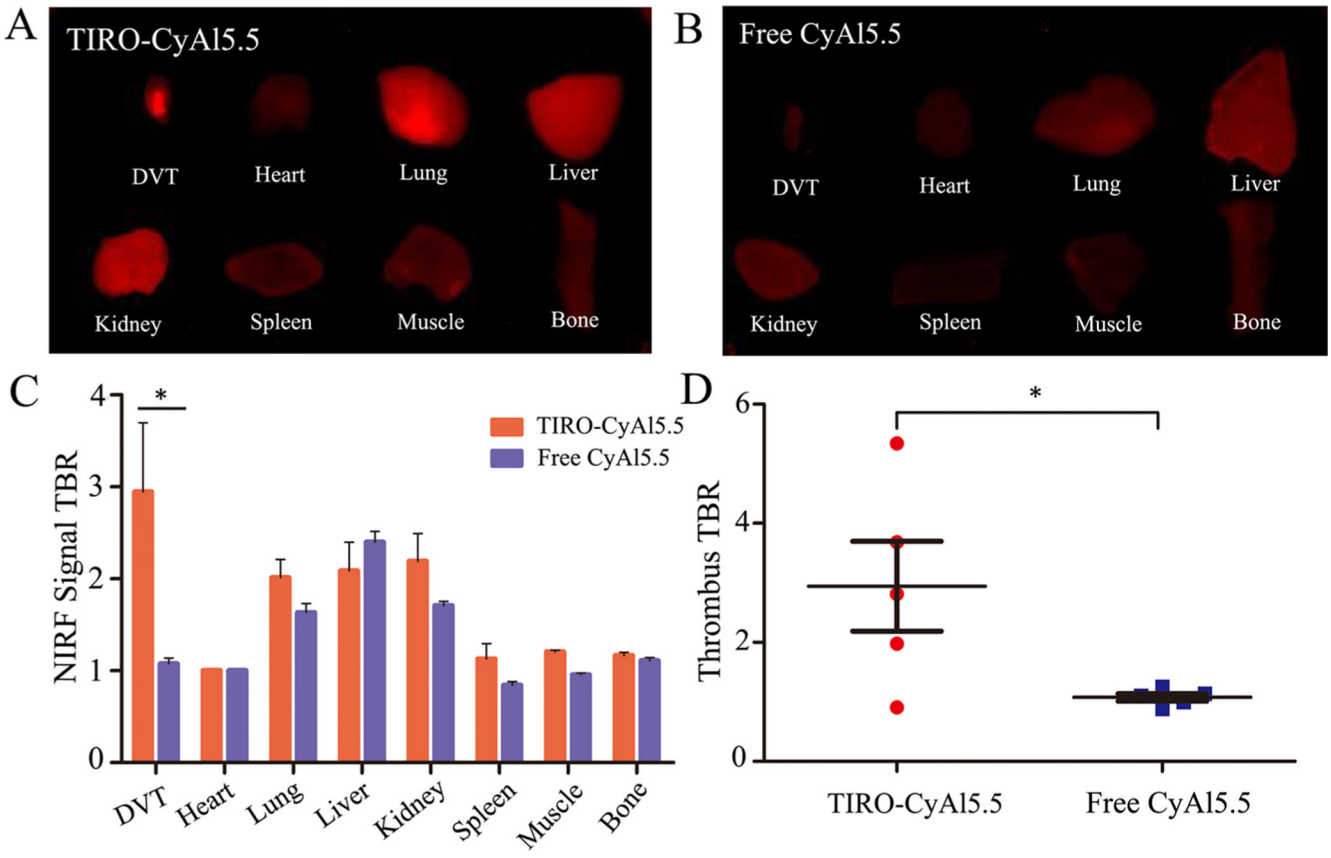

Figure 3.

In vivo biodistribution of TIRO-CyAl5.5. (A,B) Representative NIR fluorescence images of *ex vivo* organs harvested 30 min after intravenous administration of the indicated contrast agent. (C) Quantitative summary of fluorescence intensity of organs collected 30 min after intravenous administration of the TIRO-CyAl5.5 and free CyAl5.5, where bars represent the average (TBRs; mean ± SD) of $N = 5$ mice. (D) Administration of TIRO-CyAl5.5 resulted in a 2.74-fold increase in the jugular vein thrombus signal compared to free CyAl5.5. $*P < 0.05$.

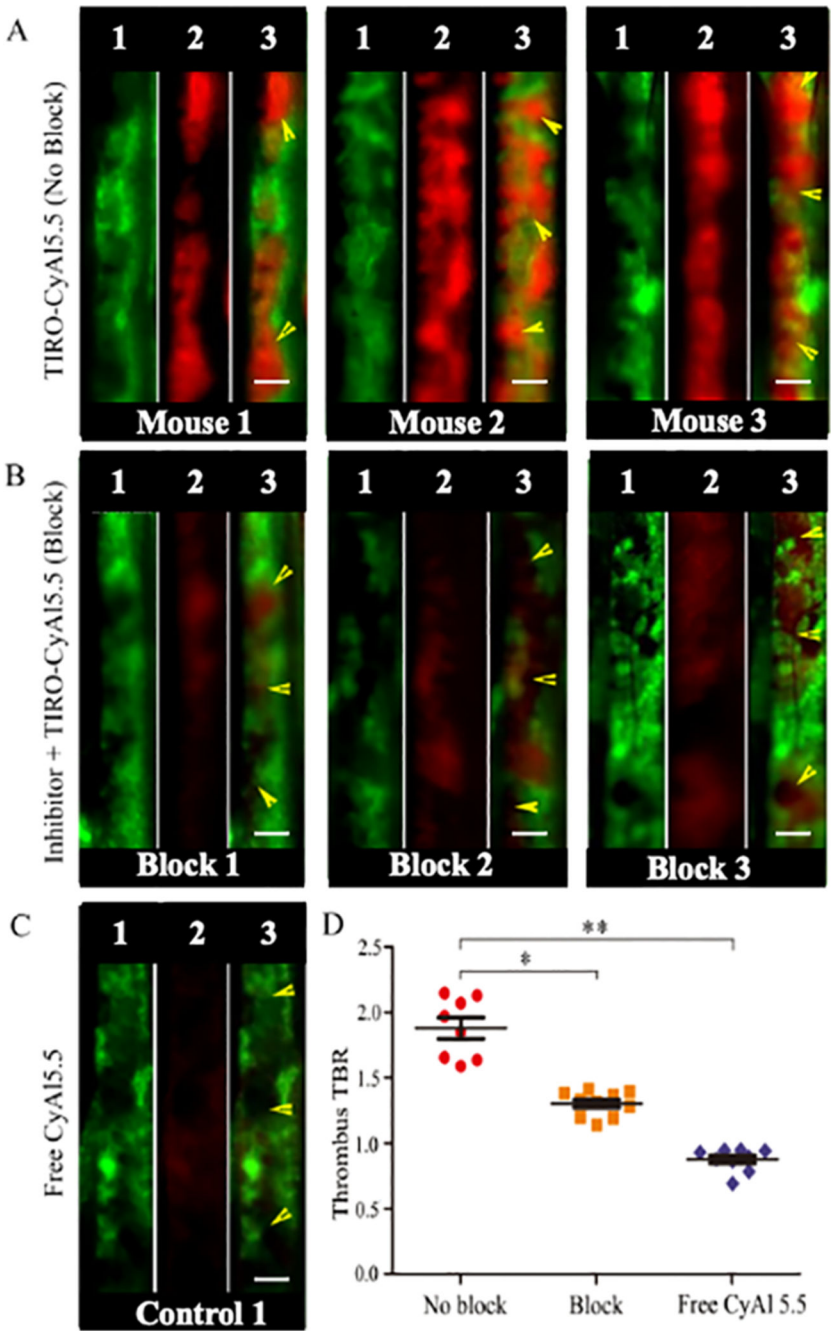

Figure 4.

High-resolution IVFM detection of platelet deposition in murine femoral venous thrombosis *in vivo*. Mice received either (A) TIRO-CyAl5.5 “no block,” (B) a 2500-fold excess of unmodified tirofiban to saturate GPIIb/IIIa receptors, followed by TIRO-CyAl5.5 “block,” or (C) “free” CyAl5.5. (D) Quantification of the NIRF TBR signal for each of the treatment groups. Each set of three images is a separate animal in the denoted experimental group. Within each set (1) FITC-dextran-mediated angiogram, (2) signal in the CyAl5.5 channel, and (3) merged image of the two channels. *$P < 0.05$, **$P < 0.001$, scale bars, 100 μm. Yellow arrows indicate a thrombosed area per FITC-dextran-mediated angiogram.

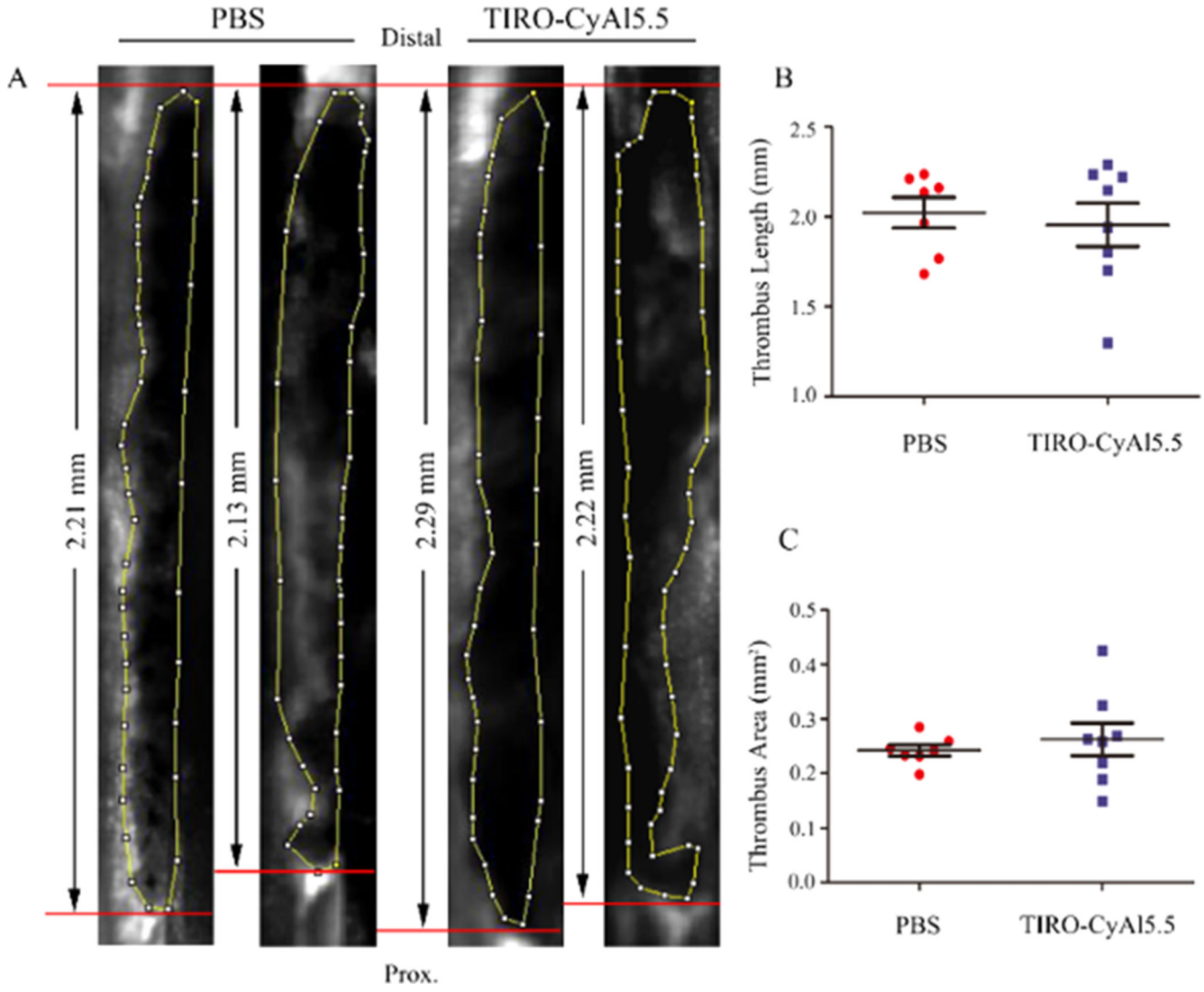

Figure 5.

Effects of the NIRF platelet imaging agent TIRO-CyAl5.5 on venous thrombus (VT) length and area. Thrombi were visualized by IVFM *via* a FITC-dextran angiogram as hypointense areas in the vein. Representative IVFM angiograms are shown in PBS- and TIRO-CyAl5.5-treated animals with 7.5% $FeCl_3$-induced DVT. Each angiogram depicts results from a different animal. (A) Thrombus length and area measurements showed no significant difference between TIRO-CyAl5.5-treated animals *vs* PBS (B,C). Bars represent mean ± SD of 7–8 animals per group.

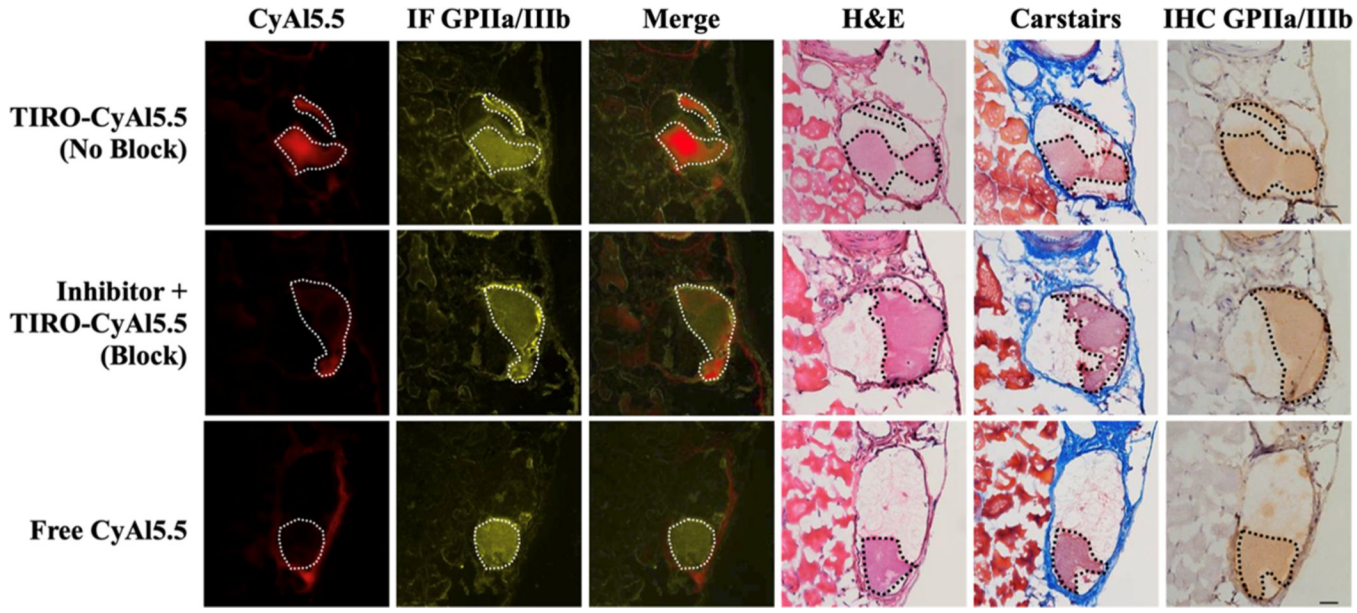

Figure 6.

Thrombus-specific binding of TIRO-CyAl5.5 in murine venous thrombi. Each group shows fluorescence microscopy, immunofluorescence (IF), immunohistochemical (IHC), Carstairs', hematoxylin, and eosin photo-micrographs. CyAl5.5 (red), IF (yellow), merged image (CyAl5.5 + IF_GPIIb/IIIa), Carstairs', hematoxylin and eosin, and IHC were shown in each group. From IF and IHC results *ex vivo*, GPIIb/IIIa expression in thrombi resected 35 min after creation. The thrombus is denoted by a dotted line. Scale bars = 100 μm.

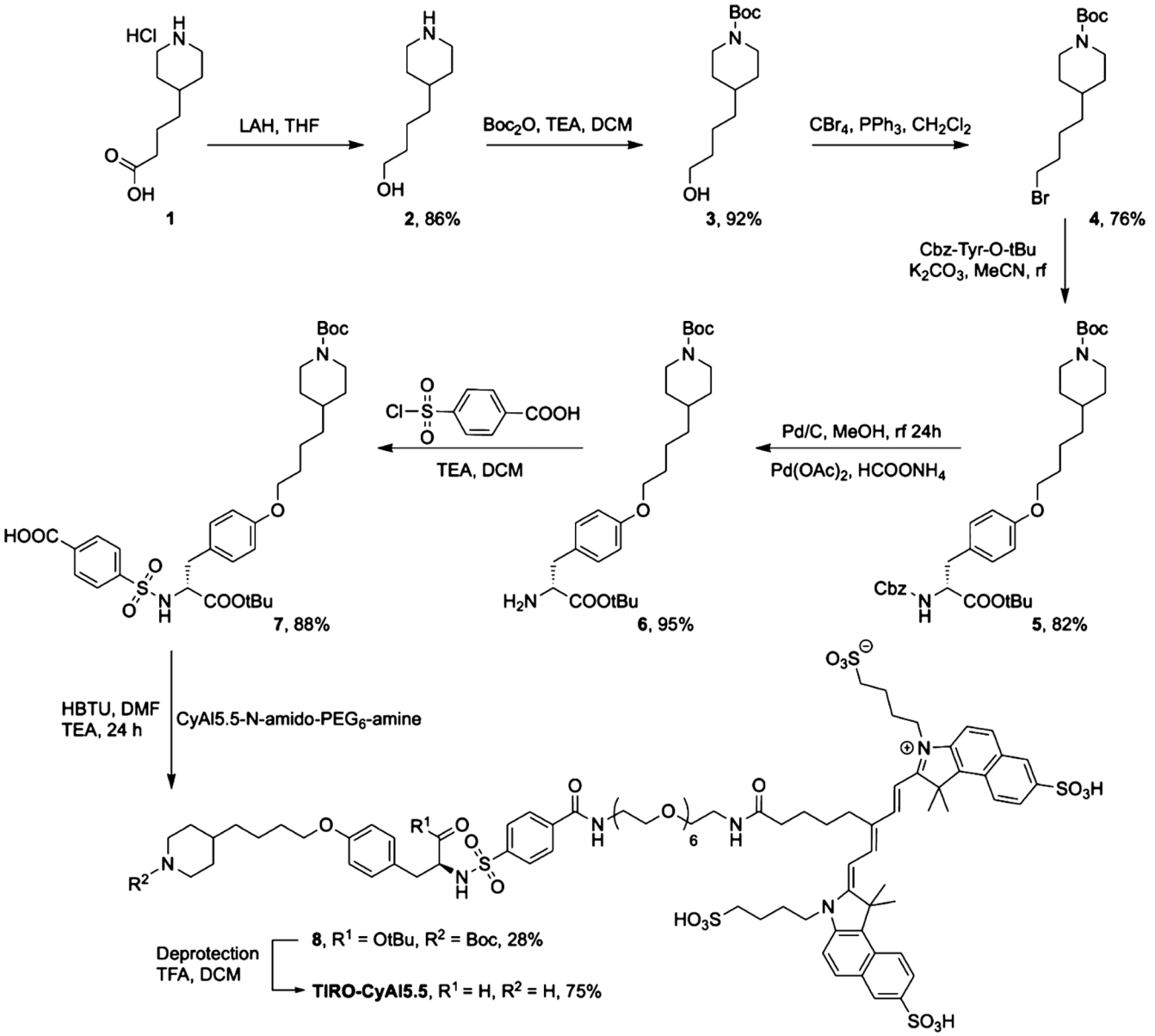

Scheme 1.
Synthesis of TIRO-CyAl5.5